

Magnetization dynamics of interacting iron nanocrystals in SiO₂

K. S. Buchanan, A. Krichevsky, M. R. Freeman, and A. Meldrum

Department of Physics, University of Alberta, Edmonton, Alberta T6G 2J1, Canada

(Received 10 March 2004; revised manuscript received 9 August 2004; published 18 November 2004)

We find that ensembles of iron nanocrystals embedded within a matrix of SiO₂ exhibit both a large Faraday rotation and ultrafast magnetic relaxation. The Verdet constant is $6.3^\circ \pm 0.4^\circ/\text{cm/Oe}$ and a still-unsaturated Faraday rotation of $3.8^\circ \pm 0.2^\circ/\mu\text{m}$ was observed at a wavelength of 532 nm for a specimen containing nanocrystals ranging up to 20 nm in diameter. The dynamic response of the nanocrystals to a transient magnetic field produced by a current pulse propagating through a lithographically patterned wire was probed using time-resolved magneto-optical Kerr-effect microscopy. The rise time of the magnetic response to a transient out-of-plane field was observed to be as fast as 26 ps. Magnetostatic interactions between nanoparticles play a significant role in determining the observed static and dynamic properties of the nanocomposite.

DOI: 10.1103/PhysRevB.70.174436

PACS number(s): 75.75.+a

I. INTRODUCTION

The magneto-optical properties of nanostructured Fe thin films are found to be different from those of bulk iron.¹ The Kerr rotation for granular films has been shown to depend on both the particle density and particle/matrix interface.² Other studies indicate that the magneto-optical properties of Fe nanocomposites agree reasonably well with effective medium approximations for particle sizes larger than 4 nm (Ref. 3). Magnetic nanoparticles may find important applications in ultra-high-density magnetic recording technologies. For individual bits with particle size and separation smaller than 50 nm (i.e., single nanoparticles) recording media with areal densities approaching 1 terabit/sq. in. might be obtained.⁴ This would represent a substantial evolution of current technology, in which the storage densities are at about 60 gigabits/sq. in. in high-end commercially available products and 100 gigabits/sq. in. in the lab.⁵ While the properties of isolated single-domain magnetic nanoparticles are reasonably well understood,⁶ the effects of interparticle interactions on the behavior of an ensemble of nanoparticles continues to be an active area of research.⁷⁻⁹ Improvements in access speed are also desirable, thus exploration of the dynamic properties of magnetic nanoparticles is relevant to the advancement of data storage technology.

In this study, the static and dynamic magnetic and magneto-optical properties of a thin layer of strongly interacting Fe nanocrystals were examined. Magnetic hysteresis curves were measured using Faraday rotation, and the dynamics of the nanocomposite were investigated using ultrafast time-resolved scanning Kerr-effect microscopy (TR-SKEM), a powerful tool that combines picosecond temporal and sub-micrometer spatial resolution.^{10,11} The TR-SKEM technique has been applied to permalloy microstructures¹² and has provided insights into magnetic switching dynamics.¹³ This technique, however, has not yet been applied to nanocomposite materials.

II. EXPERIMENTAL

The samples were prepared using ion implantation, a versatile technique for fabricating nanocomposite materials.¹⁴

Samples were prepared by implanting an optical-quality fused quartz wafer (Esco Products type A1, 1 mm thick) with 80 keV Fe ions to a fluence of 1.5×10^{17} ions/cm². The specimens were clipped into a supporting plate and were not heat sunk. The beam current was maintained at less than 25 μA in order to minimize local heating effects. Patterned arrays were also prepared by implanting ions through a Mo mask with 5 and 10 μm square holes.¹⁵ These patterned samples allow for convenient differentiation between signals arising from the matrix and the nanocrystals when using scanning microscopy techniques. Thermal annealing is often used to modify the properties of ion-implanted materials; in most cases it promotes aggregation and growth of nanocrystals. The sample concentrated on here, however, was found to contain nanocrystals directly after implantation and was examined in its as-implanted state. The microstructure of the sample was characterized using transmission electron microscopy and electron diffraction. The optical reflectivity, transmission, and absorbance were measured using a fiber optic spectrometer.

Magnetic hysteresis loops were measured using Faraday rotation, a technique that works well for these semitransparent ion-implanted samples. Polarized light traveling through the sample undergoes a rotation in polarization proportional to the magnetization component parallel to the direction of propagation.¹⁶ The rotation was measured using a rotatable analyzer set a few degrees from the extinction point in order to maximize the signal-to-noise ratio. A differential detection scheme, which rejects common-mode laser noise, was used to record the signal in transmission.¹⁷ For in-plane measurements, the beam was incident at an angle of 22° in the longitudinal configuration and a polar arrangement with normal incidence was used for the out-of-plane measurements.

Figure 1 shows a cross-sectional view of the sample position with respect to lithographically patterned write wires. The U-shaped gold write wires used here were 10 μm in width, separated by 10 μm . They were fabricated by first sputtering 30 nm of titanium followed by 300 nm of gold onto a sapphire substrate. The wires were then patterned using standard deep UV lithography and wet etching techniques. Small aluminum mirrors, 10 nm thick and $\sim 10 \mu\text{m}$ on a side, were similarly fabricated on the implanted surface

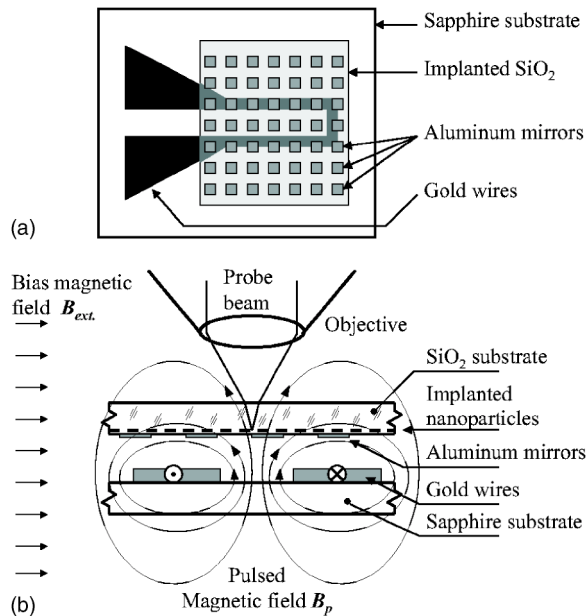


FIG. 1. Diagram showing the transmission wire layout in (a) plan view and (b) in cross section. Gold write wires (300 nm thick) are patterned on a sapphire substrate. Nanocomposites are formed in a separate (transparent) substrate and 10 μm aluminum mirrors are patterned on the implanted surface, which is then positioned directly on top of the write wires. A current pulse traveling through the wires generates a magnetic field that is oriented in-plane over the wires and out-of-plane between the wires. Polarized light is focused on the sample surface and used to probe the magnetization state.

of the nanocomposite specimen, which was then mounted directly on top of the write wires. We estimate the spacing between the nanocrystals and the write wires to be a few micrometers based on the difference in focus distance for the gold wires and mirrors patterned on the implanted face of the nanocomposite specimen.

In order to quantitatively characterize the dynamic magnetic response of the sample we used time-resolved scanning Kerr microscopy.¹⁸ This stroboscopic pump-probe method locally probes the change in all three components of the magnetization. The probe beam (mode-locked Ti-sapphire beam, wavelength 800 nm, repetition rate of 740–760 kHz, average power between 20 and 40 μW) was focused using an objective lens through the silicon dioxide substrate onto the layer of implanted nanoparticles. The focused laser spot size was estimated to be 1.2 μm . The objective was mounted on a precision translation stage, allowing it to move through a range of 20 μm , forming a scanning optical microscope. The nanocrystal specimen is more transmissive than reflective, thus, the signal from the mirrored areas, which arises from twice the single-pass Faraday rotation reduced slightly by the weaker Kerr signal, is stronger than the signal obtained from areas of the sample not positioned over reflective elements. Signals were compared for the probe beam focused at the active layer atop or between the mirrors, directly above the write wires, or between them. Patterned samples with mirrors over both the 5 by 5 and 10 by 10 μm^2 implanted regions and nonimplanted regions were also examined.

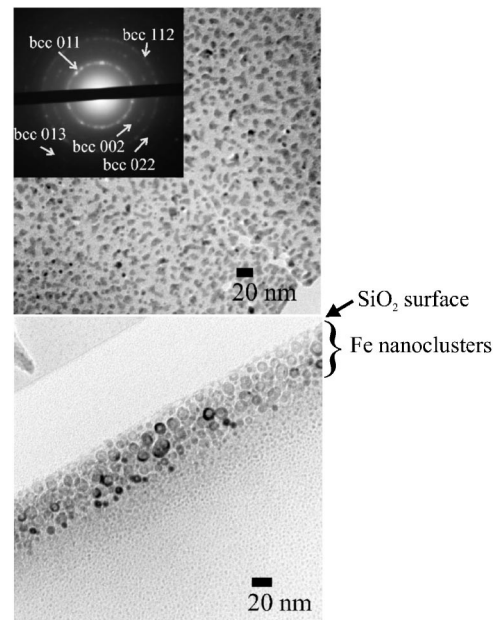


FIG. 2. Plan view (top) and cross-sectional (bottom) TEM micrographs of Fe nanoclusters in SiO_2 . Fe ions (80 kV) were implanted to a fluence of 1.5×10^{17} ions/ cm^2 into the SiO_2 substrate, which was held at room temperature during implantation. This sample was not annealed. The Fe nanoclusters are located within 60 nm of the sample surface.

The magnetization state of the specimen was modulated by the magnetic field created by current pulses propagating down the write wire. The corresponding pulsed magnetic field is predominantly an in-plane field over the wire and an out-of-plane field between the wires. In this experiment we used several different pulse source/delay line combinations. The first was a 50 V pulser with a 250 ps rise time (Picosecond Pulse Labs 2000D Turbo) in combination with an electronic delay line with a characteristic jitter of 220 ps. The second was a 10 V pulser with a 50 ps rise time (PSPL 4050B) in combination with an optical delay line. The first setup provides a stronger signal and a longer scan range of 120 ns, while the second setup has better temporal resolution but is limited to shorter 4 ns scans and weaker magnetic field pulses. The temporal resolution can be further improved by using an optical pulse to excite a biased photoconductive switch, which provides a current pulse with a rise time of only a few picoseconds.^{12,19} In all cases, constant in-plane bias magnetic fields ranging from 0 to more than 1 kOe were applied.

III. RESULTS

A. Sample characterization

Transmission electron microscopy (TEM) was performed on the ion-implanted sample, in both the plan view and cross-sectional modes. Bright field images of the as-implanted sample show spherical nanoclusters of iron with mean diameters of about 10 nm concentrated within the top 62 ± 2 nm of the specimen (Fig. 2). This estimate for the

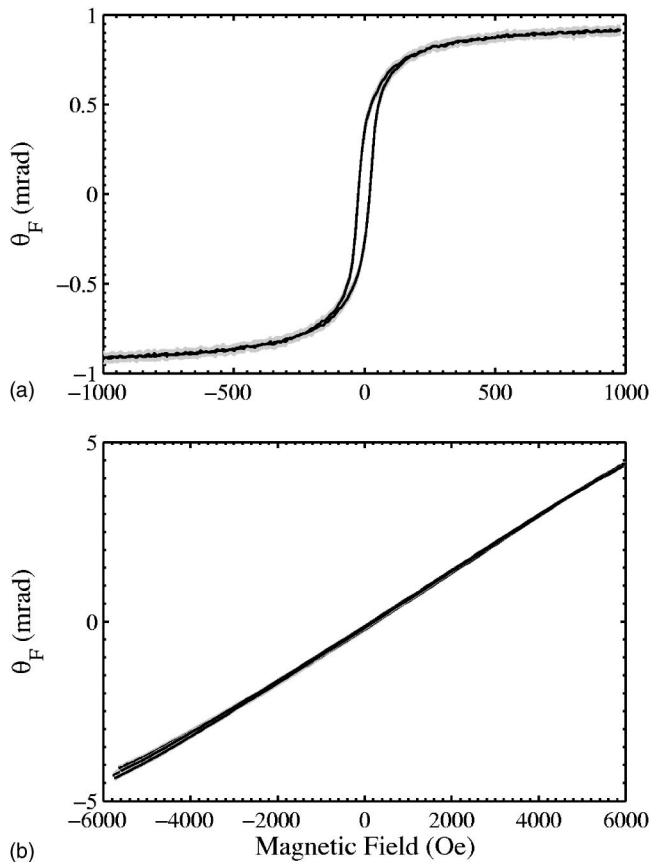


FIG. 3. In-plane (a) and out-of-plane (b) magnetic hysteresis curves for the Fe implanted SiO_2 sample obtained at room temperature through Faraday rotation.

implanted layer thickness is representative of the thickness of the layer where the majority of the larger nanocrystals are concentrated as measured from cross-sectional TEM micrographs. The filling factor is estimated to be $35 \pm 5\%$ based on examination of thin areas of the plan view specimen. Electron diffraction measurements reveal the presence of crystalline iron in the bcc (ferromagnetic) form.

B. Static Faraday hysteresis

The hysteresis loops for the Fe implanted SiO_2 sample are shown in Fig. 3. A correction was made for the Faraday rotation in the SiO_2 host, which was first thinned to $205 \pm 5 \mu\text{m}$ to reduce this contribution. A magnetic field of more than 400 Oe in the in-plane direction is needed to fully magnetize the sample and the in-plane coercivity is 23 ± 5 Oe, indicating that the blocking temperature for this nanocomposite is above room temperature. The out-of-plane hysteresis loop for the same sample is shown in Fig. 3(b). No coercivity is observed within the resolution of the measurement, and the maximum magnetic field (6 kOe) is not sufficient to saturate the sample.

The Faraday signal from this sample is large, with a Verdet constant (out-of-plane configuration) of $6.3 \pm 0.4^\circ/\text{cm}/\text{Oe}$ measured at a wavelength of 532 nm. Part of the uncertainty of this measurement is attributed to

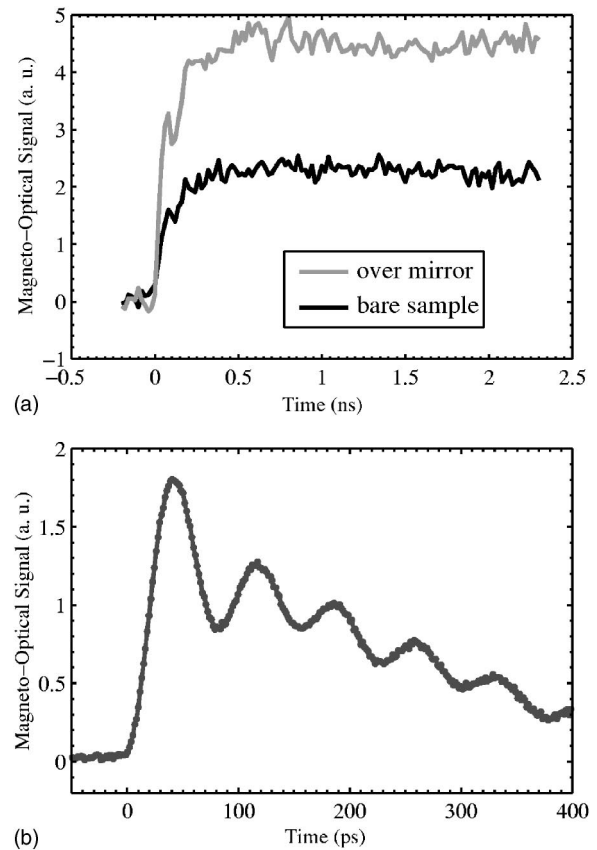


FIG. 4. (a) Kerr vs Faraday magneto-optical signal from the implanted nanoparticles in response to a transient out-of-plane field generated by an electronic pulser (square pulse). The stronger Faraday signal (gray line) has opposite polarity as compared to the Kerr signal and has been inverted to allow for direct comparison. (b) The magneto-optical response to a current pulse generated using a photoconductive switch (fast ~ 1 – 10 ps rise, exponential decay), for zero bias field.

statistical fluctuations in the rotation measurement, and there is also some uncertainty in defining the exact thickness of the implanted layer. For an applied field of 6 kOe, a Faraday rotation θ_F (as compared to zero field) of $3.8^\circ \pm 0.2^\circ/\mu\text{m}$ was observed. The Faraday rotation for bulk iron is $7.8^\circ/\mu\text{m}$ based on the optical²⁰ and magneto-optical²¹ parameters for $\lambda = 532$ nm.

The absorption—another property that is important when considering a material for magneto-optical applications—was also measured. At a wavelength of 532 nm the nanocomposite was found to be 38% transmissive and 28% reflective, which corresponds to an absorption coefficient of $10.3 \pm 0.8 \mu\text{m}^{-1}$. The absorption is lower at 800 nm ($6.5 \pm 0.3 \mu\text{m}^{-1}$) than it is for the visible spectrum. For bulk iron, the absorption for $\lambda = 532$ nm is $79 \mu\text{m}^{-1}$, which is larger than that of the nanocomposite.²⁰

C. Dynamic measurements

Magnetodynamic measurements were made on the Fe implanted SiO_2 sample. The out-of-plane response to a square-pulse excitation [Fig. 4(a)] was measured first using the 50 V

pulser/electrical delay line combination (not shown) and then using the 10 V pulser/optical delay line combination (pulse amplitude approximately 80 Oe). In both cases the response followed the profile of the current pulse and was sufficiently fast that the measurement was limited by the rise time of the current pulse. In addition, the shape of the response was unaffected by the presence or absence of an in-plane bias field of >1 kOe. A spatially uniform response was observed within the resolution limits of the system for both the patterned and bulk implanted samples. Measurements of the patterned implanted samples confirm that the signal is spatially correlated with implanted areas and there is no signal from the host material.

In this particular semitransparent sample (48% transmissive, 28% reflective at $\lambda=800$ nm), the magneto-optical response is a combination of Kerr and Faraday effects for reflected and transmitted light, respectively. In order to demonstrate the effect of Faraday rotation as compared to a Kerr polarization shift, the beam was focused on the layer of implanted nanoparticles on top of an aluminum micromirror and the signal was compared to the magneto-optical response at a point adjacent to the mirror. Figure 4(a) shows a comparison of these responses in the absence of any bias magnetic field.

The black curve represents the Kerr signal from the bare sample. The magneto-optical rotation measured from the mirror region was approximately double that reflected from only the nanoparticles, and the rotation was also opposite in direction. The polarized beam incident on the mirrors travels twice through the nanocomposite, resulting in double the Faraday rotation, but the overall signal is reduced by the Kerr effect originating from the portion of the beam that is reflected directly by the nanocomposite and through absorption. Henceforth these effects will be referred to simply as magneto-optical effects, since the same underlying physics applies whether the light is reflected or transmitted.

The magneto-optical response recorded over the mirrors is very similar in shape (within the noise level) as compared to the signal measured from the bare nanocomposite. For both samples, the time it takes to reach the maximum change in magnetization is around 150 ps (measured from 10 to 90% of the maximum amplitude). The apparent rise time of the pulse has been degraded by a reflection from impedance mismatched short indium wires connecting the lithographic line to a 50 Ohm coaxial cable.

The out-of-plane measurements were repeated using photoconductive switches to obtain a faster measurement of the response time of the nanocomposite to an out-of-plane excitation [Fig. 4(b)]. The polar Kerr signal follows the expected pulse shape with low-amplitude oscillations superimposed. The rise time for the zero bias field is 26 ± 1 ps, limited by the material. The response is similar for bias fields up to 1.7 kOe with rise times ranging from 26 to 44 ps. A self-consistent effective medium theory³ for iron spheres in SiO₂ ($\eta=1.46$) yields 5 mrad as an estimate for the magneto-optical rotation from the bare nanocomposite for a wavelength of 800 nm. For a typical photoconductive switch measurement, the maximum observed Kerr rotation was approximately 0.0080 mrad for an excitation of at least 7 Oe in amplitude. Using these values, the maximum out-of-plane tilt is estimated to be only 0.16% (0.09°).

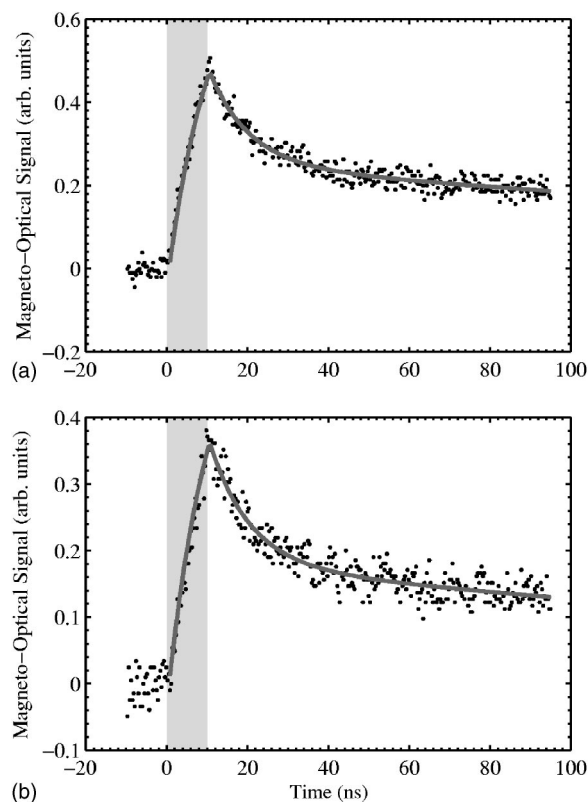


FIG. 5. In-plane response of the Fe implanted SiO₂ to a magnetic field generated by a 10 ns, 1 A current pulse (shaded region) in the presence of (a) zero in-plane bias field, and (b) a 250 Oe in-plane field. Solid lines show a two-exponential fit to data after the falling edge of the pulse.

For transient magnetic fields applied in the plane of the sample, a much different response is observed. The magnetic response to a square-pulse excitation (the magnitude is 600 Oe directly over wire and approximately 150 Oe $10 \mu\text{m}$ above the wire) is relatively slow (Fig. 5). The x (in-plane, perpendicular to the direction of current flow) magnetization component changes almost linearly from the time that the magnetic pulse begins until it ends (10 ns). Once the transient pulse ends, the magnetization of the sample slowly relaxes back to its original state over the course of more than 80 ns. Data taken with bias fields ranging from 0 to 200 gauss show the same behavior.

Focusing in on the data starting from the end of the transient pulse, a two-exponential function $f(t)=A_1 \exp[-(t-t_2)/\tau_1]+A_2 \exp[-(t-t_2)/\tau_2]$, where t_2 is the end-time of the pulse, provides a good fit. This function was chosen because the slow relaxation of the magnetization back to equilibrium appears exponential in nature, but is not well described by a single time constant. A standard nonlinear least-squares fitting method was used (Gauss-Newton method), yielding the values for the two time constants and the ratio of the amplitude constants shown in Table I. The fit parameters for both the data taken at zero bias field and a bias field of 200 Oe agree within error; both exhibit a relatively fast relaxation of $\tau_1=10$ ns and a slower time constant of $\tau_2 \approx 300$ ns. Exponential behavior also agrees with the data taken over the duration of the pulse. Here, the time constant

TABLE I. Exponential fit parameters for in-plane temporal data. Uncertainties represent a 95% confidence interval on the fitting parameters.

Bias Field (Oe)	τ_1 (ns)	τ_2 (ns)	A_1/A_2
0	10 ± 2	280 ± 80	0.88 ± 0.09
200	10 ± 2	300 ± 100	1.0 ± 0.1

τ_1 found for the falling edge provides a good match to the data taken during the pulse when substituted into the function $f(t) = (A_1 + A_2) \{ 1 - \exp[-(t - t_1)/\tau_1] / (1 - \exp[-(t_2 - t_1)/\tau_1]) \}$, where t_1 is the pulse-on time. The duration of the pulse is short compared to τ_2 , thus adding the second exponential term makes no difference in the quality of the fit to the data during the pulse.

To summarize the results of the dynamic measurements, the ensemble of iron nanocrystals responds very slowly to both the leading and falling edges of an in-plane transient magnetic field pulse. In contrast, the nanocomposite shows a very fast response to an out-of-plane magnetic field. For both the in-plane and out-of-plane measurements using electronic pulsers, the shape of the temporal response was found to be independent of the magnitude of an in-plane bias field. At faster time scales the overall character of the out-of-plane response does not change with bias field, however, the rise time of the response and frequency of the superimposed oscillations do vary. For the in-plane measurements, the maximum field applied was 200 Oe; for the out-of-plane measurements higher fields of up to 1.75 kOe were applied.

IV. MICROMAGNETICS SIMULATIONS

A. Simulation models and parameters

Micromagnetic simulations have been carried out on simplified models of the nanocomposite system in order to gain insight into the origins of the vastly different responses according to orientation of the transient magnetic field. Simulations were carried out using the LLG Micromagnetic Simulator^{TM,22}. The sample was approximated as an array of ferromagnetic particles arranged on a plane. Simulations were carried out for a variety of models involving regular and random arrays of cubic and cylindrical arrays of nanoparticles, but only the results for the simulation most closely modeled on the real nanocomposite will be presented here.

The sample was modeled using randomly placed 10 nm cubes on a 2.5 nm by 2.5 nm grid (256 by 256 elements) with a minimum separation of 2.5 nm [Fig. 6(a)], corresponding to a filling factor of approximately 40%. Each particle is therefore described by 16 cells that are 10 nm thick. Cubic crystalline anisotropy was imposed with the anisotropy axes aligned along the principle axes of the cubes. Assigning random anisotropy axes to each particle would be a better representation of the specimen, but is difficult to impose in the software package used. Also, the anisotropy energy is an order-of-magnitude smaller than the demagnetization energy, therefore, the crystalline anisotropy is not expected to be the primary factor in determining the response

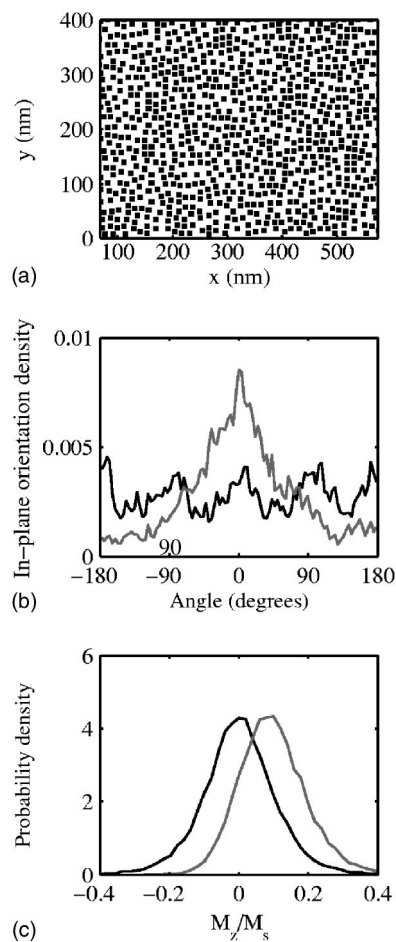


FIG. 6. Simulation results for a random array of 10 nm cubes with cubic anisotropy imposed and no bias magnetic field. (a) The model used in the simulations where the black areas are magnetic (only part of the model is shown). (b) Histograms of the in-plane angle of the magnetization before (black) and at 0.6 ns after the onset of a transient in-plane magnetic field pulse (gray). (c) Corresponding histograms of the out-of-plane component of the magnetization M_z before (solid black line) and 0.6 ns after the onset of a transient out-of-plane magnetic field pulse (gray line). In both cases the magnitude of the transient magnetic field was 600 Oe.

of this model. The magnetic constants for bulk iron were used in the simulations ($M_s = 1714 \text{ emu/cm}^3$, $K_1 = 4.7 \times 10^5 \text{ erg/cm}^3$, exchange energy $2.1 \times 10^{-6} \text{ erg/cm}$). The particles in the model are exchange decoupled through physical separation, but are close-enough together that dipolar interactions are very important.

A stable initial state was found by allowing the array of particles to relax to its equilibrium state from a random state; that is, a state where each grid cell is assigned a random magnetization orientation in three dimensions. Separate initial states were found for each static magnetic bias field. To model the response to a transient field, the model in its initial state was subjected to a fast magnetic field pulse approximating the output of the electronic pulse generator used in the experiments: the fast edge rises from zero to the saturation level in 60 ps, remains constant for 10 ns, and then drops to zero in 1 ns. Pulses of up to 600 Oe in amplitude were simu-

lated, applied in the x and z directions. For the out-of-plane simulations the pulse duration was reduced from 10 to 5 ns to save on computational time, and the simulations were also carried out using the function $\vec{h}(t) = h_{max}[1 - \exp(-t/\tau_r)]\exp(-t/\tau_c)\hat{k}$ to approximate the profile of the pulse generated by the photoconductive switch (pulse rise time $\tau_r = 1$ ps, carrier lifetime $\tau_c = 250$ ps). In addition to the temporal response simulations, hysteresis curves were also mapped out by allowing the model to relax in sequentially applied static fields.

B. Simulation results and discussion

The model used to approximate the specimen is shown in Fig. 6(a). This figure also shows histograms of the distributions of in-plane angles (b) and M_z/M_s values (c) in response to in-plane and out-of-plane transient fields, respectively. The black curves show the distributions for the initial state (before the onset of the transient pulse) while the gray represents the distribution observed during the transient magnetic field pulse (0.6 ns after the pulse onset). For the initial state (black curves in Fig. 6), the M_z distribution is narrow and is centered on zero. In contrast, the in-plane angle distribution is relatively flat with peaks along the grid/anisotropy axes. In general, the initial state for this model is predominantly in-plane with preferred in-plane orientations corresponding to the direction of any applied bias field (only the zero bias case is shown) and in the directions of the crystalline anisotropy axes.

When the transient field is applied in the in-plane direction, the M_z distribution changes very little while the in-plane angle distribution reveals an increase in alignment of the magnetization along the direction of the in-plane component of the applied field (x axis). In response to a transient out-of-plane magnetic field, the M_z distribution, which is initially centered on zero, shifts slightly in the direction of the transient field while the in-plane angle distribution remains the same. The distributions observed during the transient magnetic fields are insufficient to achieve full alignment in either case.

Figure 7(a) shows the out-of-plane temporal response (solid) to a square-wave transient field of 200 Oe applied in the out-of-plane direction. The z component of the magnetization retraces the ideal field pulse profile. The noise is random (irreproducible from run to run) and would be expected to average out in a stroboscopic experiment, which explains why the experimental measurements showed a cleaner response as compared to the simulated response to a single pulse shown here. When a transient magnetic field is simultaneously applied in the x direction ($H_x = H_z = 200$ Oe, $H_y = 0$ Oe), the M_z response is almost identical (not shown). These results suggest that the fast out-of-plane response is governed by collective small-angle (and thus linear in field strength) tilt of mostly in-plane magnetized particles and is virtually decoupled from the slow, large-angle in-plane switching of individual particles. This out-of-plane response is unaffected by the presence of static in-plane bias fields of 200 Oe or 1.75 kOe at this time scale (not shown).

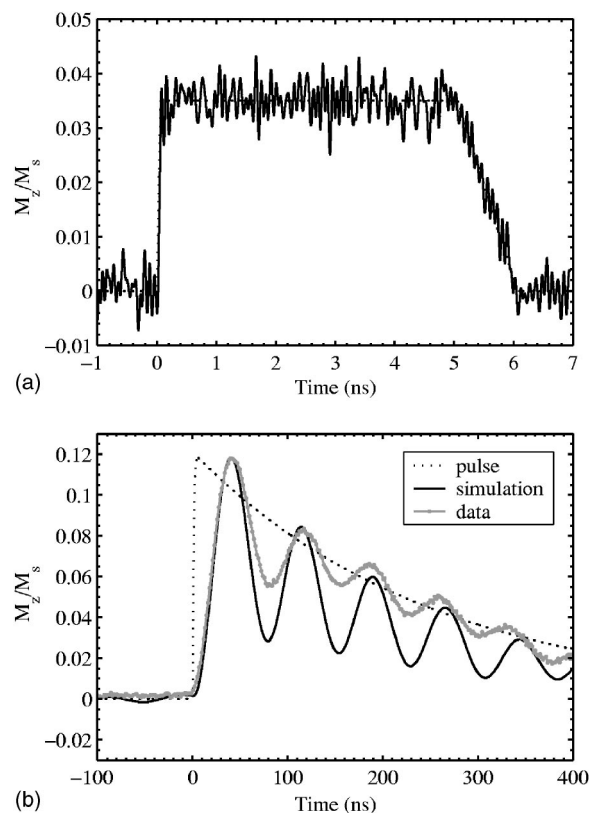


FIG. 7. Simulated out-of-plane magnetization M_z response (solid) for an irregular array of cubes averaged over the entire array as a function of time. In (a) a 5 ns pulse was applied in the z direction with a maximum amplitude of 200 Oe, while in (b) a pulse meant to approximate that of the photoconductive switch was used. The magnetic field pulse profiles are shown schematically as a dotted line and in (b) the data have also been included (scaled to match the amplitude of the simulated magnetization response).

The M_z temporal response of the model to a photoconductive-switchlike pulse is shown in Fig. 7(b) for zero bias field. For this particular simulation a saturation magnetization of $M_s = 1350$ emu/cm³ was used to obtain a similar rise time to the data. Overall the response follows the shape of the pulse with oscillations superimposed that are slightly larger in magnitude than those observed experimentally. Adding an in-plane bias field results in a similar response but with small changes in the rise times and oscillation frequencies. Examination of the responses of the individual particles reveals that they oscillate such that, on average, the particles tilt out of plane by a small amount, with the result that the M_z response follows the shape of the transient field. The in-plane components of the oscillations cancel out resulting in zero net in-plane response at zero bias field. These oscillations are much lower in amplitude and are damped more quickly than would be expected for a continuous thin film. Simulations carried out using the same parameters but with the array replaced with an iron thin film of the same size yields a response with higher oscillations that do not damp appreciably over the course of 400 ps. The thin-film simulations, however, do yield a similar response if the damping parameter is increased from 0.0023 to 0.05, suggesting that this nanocomposite has an effective damping

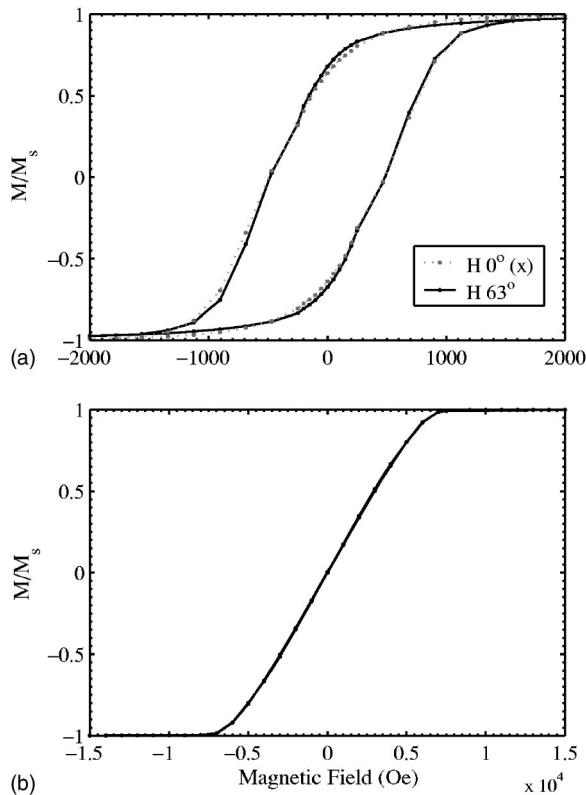


FIG. 8. Simulations of the (a) in-plane hysteresis curves along the x -direction (easy axis of cubes) and at an angle of 63° in-plane, and (b) out-of-plane hysteresis curve for an irregular array of 10 nm cubes, 2.5 nm minimum separation (40% fill factor). The individual points show the actual simulation results while the connecting lines are meant as a guide to the eye.

parameter that is approximately 20 times larger than that of bulk iron.

Simulated in-plane hysteresis curves are shown in Fig. 8(a). These curves were simulated with the magnetic field applied along the x -axis (easy axis of the cubes) and at an in-plane angle of 63° . The curves differ significantly from those of a single 10 nm cube, which are square in shape with coercivities of approximately 500 (0°) and 175 Oe (63°). For a random array of particles, the coercivity is reduced (slightly less than 500 Oe), the curves are rounded rather than square, and the in-plane response is close to being isotropic. In these simulations, the anisotropy energy (only from crystalline anisotropy) is almost two orders-of-magnitude smaller than the demagnetization energy, which helps to explain the change from anisotropic to isotropic behavior. These effects agree with previous simulation results.⁸ The out-of-plane hysteresis curve [Fig. 8(b)] is linear up to an applied field of approximately 6 kOe, which is consistent with the measured out-of-plane hysteresis response. The coercivities of the models are larger than that of the nanocomposite specimen, but the shapes of the curves are similar.

Figure 9 shows the in-plane magnetization response (M_x) as a function of time for the model in zero bias field. For these simulations, transient magnetic field pulses of 60 and 600 Oe were applied in the x direction. The 60 Oe pulse simulations have been scaled by a factor of 10 so that the

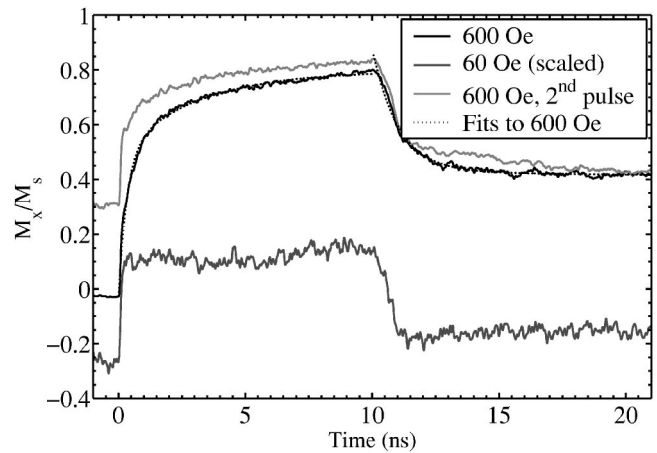


FIG. 9. Average in-plane magnetization M_x as a function of time for the model in response to in-plane transient magnetic fields (x direction) of 60 and 600 Oe. The curve labeled “600 Oe, 2nd pulse” is the response of the final state in the 600 Oe pulse simulation to a second pulse of the same magnitude. The 60 Oe results have been scaled so that the shapes of the responses can be compared more easily. Two-exponential fits to the 600 Oe simulation results during and after the pulse are also shown.

shapes of the responses can be more easily compared on the same plot. The response to the 60 Oe pulse, which is significantly smaller than the coercivity of this model, is more similar to the observed out-of-plane response rather than the in-plane response in that it mirrors the pulse shape. The response to the 600 Oe pulse, which is larger than the coercivity of the model, is smoother with an initial fast response followed by a slower approach to saturation during the pulse. The effect of an in-plane bias field of 200 Oe applied antiparallel to the transient field was also explored for a 600 Oe transient pulse. The shape of the response during the pulse was found to be unaffected by the bias field, however, the simulation with the 200 Oe bias field showed a slightly steeper approach to equilibrium on a relative scale for the same excitation magnitude. The time-resolved measurements rely on repetition of the excitation. To explore the effect of having a nonequilibrium initial state, the simulation was repeated using the final state ($t=21$ ns) from each simulation as the initial state in an identical simulation, which yielded very similar response shapes for both the 60 and 600 Oe pulse amplitudes.

Qualitative features of the 600 Oe simulations are in agreement with the experiment. The simulations yield a fast initial response followed by a slower approach to saturation during the pulse. Similarly the relaxation to the initial state after the pulse shows a fast initial fall in M_x followed by a slower approach to equilibrium. Both responses are, however, much faster than observed experimentally. In fact, the data taken over the full duration of the pulse were found to be well described by a single exponential function, which is believed to be analogous to the faster initial response of the model. The two-exponential function used to fit the data also describes the simulation results well (dotted lines in figure). The parameters found for fits to the results obtained during and after the pulse are shown in Table II. The fit to the

TABLE II. Exponential fit parameters for simulated response to a 600 Oe in-plane transient magnetic field. Uncertainties represent a 95% confidence interval on the fitting parameters.

	τ_1 (ns)	τ_2 (ns)	A_1/A_2
During Pulse:	0.336 ± 0.001	3.03 ± 0.02	1.706 ± 0.005
After Pulse:	1.022 ± 0.006	430.7 ± 0.9	0.937 ± 0.007

trailing edge is not as good as the fit during the pulse because the initial fall of the simulation is actually limited by the 900 ps fall time of the pulse. The fit parameters for the results during and after the pulse are different, especially for τ_2 . If the pulse fall time is limited to 60 ps, then τ_1 for the fall is comparable to τ_1 during the pulse, which is consistent with the experimental observations. The time constants from the simulations are all faster than those obtained from the experiment with the exception of τ_2 from the falling edge, which is the same order of magnitude as τ_2 from the experiment. The amplitude ratios are greater than or slightly less than 1 for the simulations and equal to or slightly less than 1 for the experiment.²⁷

The two exponential terms could be related to either two separate populations that relax with separate time constants or two separate behaviors that dominate at different time scales. The amplitude ratio would represent the relative sizes of the populations in the first case and would be related to the cross-over point in the second. With the simulations there is evidence that the states oriented initially along the positive or negative y directions respond more quickly at the onset of the pulse and level off at a lower mean M_x value. The states oriented initially along the x -axis, in contrast, are slower to respond initially and show a steeper M_x slope toward the end of the pulse. The behaviors of the two populations, however, are not different enough from each other to match the individual terms of the exponential fit. It is thus thought to be more likely that the exponential terms are related to different processes rather than different populations. At fast time scales, the onset or removal of the pulse triggers large-angle rotations of the magnetization. At longer time scales, the particles exhibit smaller angle oscillations as they settle into a more stable magnetization state.

We emphasize that the model presented here represents the physical specimen very qualitatively. The grid spacings used here are comparable to the particle sizes, which result in discrete rather than smooth variations of interparticle spacing. Also, the model shown here is for particles of uniform size while the specimen contains a distribution. The true shapes of the nanoparticles are also not well represented in the models. The in-plane magnetization change may be a manifestation of a more complex three-dimensional switching scenario.

Other models were explored, including regular arrays of 10 nm cubes under a variety of separations (2.5–15 nm edge-to-edge separation, which results in filling factors of between 64% and 16%) and in-plane bias fields, 30 and 20 nm diameter disks, cylindrical within the limits of a 5×5 nm grid with a small distribution in size (radii distribution of 7.5 and 1.5 nm, respectively) and no crystalline an-

isotropy (both random and almost regular arrangements, filling factors of 25% and 59%). The cylindrical shape is a step closer to capturing the spherical shape of the particles without significantly increasing the computational expense. In all cases, the fast out-of-plane response was reproduced and found to be decoupled from a slower in-plane response.

V. DISCUSSION

The Faraday signal from this material was found to be quite large with a Verdet constant of $6.3^\circ \pm 0.4^\circ / \text{cm/Oe}$ at a wavelength of 532 nm. For an applied field of 6 kOe, a Faraday rotation θ_F (as compared to zero field) of $3.8^\circ \pm 0.2^\circ / \mu\text{m}$ was observed, which is almost as large as that of bulk iron ($7.8^\circ / \mu\text{m}$ at saturation). Using a self-consistent effective medium theory,³ the Faraday rotation for the nanocomposite is expected to be $\phi_{iF} = 6.3^\circ \pm 0.6^\circ / \mu\text{m}$, which is slightly larger than the observed (but unsaturated) value. This can be compared to the Faraday rotation for yttrium iron garnet (YIG), a material commonly used for magneto-optical application, which is $0.0240^\circ / \mu\text{m}$ for a wavelength of 1200 nm.²³ Although the Faraday rotation from the nanocomposite is large, the absorption should also be considered when evaluating its usefulness for magneto-optical applications. The figure of merit (ϕ_F / α , where α is the absorption coefficient) for the nanocomposite is $0.085^\circ \pm 0.005^\circ / \text{dB}$, which is larger than that of bulk iron $0.0227^\circ / \text{dB}$, but still smaller than that of YIG at 800 nm, which is closer to $8^\circ / \text{dB}$.²⁴

The simulations indicated that for a collection of closely spaced single-domain iron nanoparticles, the dipolar interactions between the particles have a strong influence on both the static and dynamic properties of the ensemble. The particles do not interact through exchange, as they have no nearest-neighbor contact in the model. They are also believed to be chemically isolated by the SiO_2 matrix in the real sample. The magnetization vectors lie mainly in-plane for the same reason that thin-films are magnetized in-plane, that is, to reduce the overall demagnetization energy of the specimen. This interpretation is supported by the out-of-plane hysteresis loop, where a field greater than 6 kOe is required to saturate the specimen indicating the presence of a strong in-plane anisotropy, and also by the simulations where very little out-of-plane magnetization is observed for the initial states.

The in-plane directions of the individual particles are influenced by the crystalline anisotropy and the dipolar interactions between particles. Ordered arrays of cubes tend to exhibit stripe formation to minimize dipolar energy, a phenomenon that is also observed to a limited degree in more random arrangements of cubes. In the presence of an in-plane bias field, the nanocrystals reorient preferentially along the field and the initial state remains predominantly in-plane. A field of several hundred Oersteds, however, is required to cause all of the nanocrystals to become aligned [the in-plane hysteresis curve in Fig. 3(a) requires a field much higher than the coercive field to achieve full saturation].

To visualize the fast out-of-plane response, first consider a single-domain, spherical magnetic nanoparticle aligned

along a magnetic field in the x direction. When a transient field is applied in the z direction, there is suddenly an angle between the magnetic moment of the particle and the direction of the net effective field at that particle. The particle will begin to precess around the direction of the effective field H_{eff} at a frequency ω_o proportional to its magnitude $\omega_o = \gamma H_{eff}$, where $\gamma = 1.76 \times 10^7$ Hz Oe $^{-1}$ is the gyromagnetic ratio for an electron spin (note: this expression differs for nonspherical particles²⁵). For an ensemble of noninteracting particles in this same bias field, the result should be the same—oscillations of the particles, all at the same frequency.

In the case of a collection of magnetic nanoparticles with strong dipolar interactions, the effective field experienced by a given particle is the sum of the external field and the fields generated by all of the particles in the ensemble. With the exception of very high external fields, there will be a range of effective fields present in the nanocomposite as well as a range of initial in-plane orientations. Having a range of frequencies will cause the oscillations to cancel out (on average), yielding a measure of the average magnetization for all three components. The in-plane components average to zero while the z component follows the shape of the out-of-plane transient field. At faster time scales, some frequencies are better represented than others, which results a response that contains oscillations superimposed on the pulse shape as observed in both the experiment and the simulations.

Micromagnetic simulations are able to qualitatively reproduce the ultrafast response to an out-of-plane transient pulse and suggest that this fast out-of-plane response should exist for strongly interacting, exchange decoupled nanoparticle arrays in general. For this specimen, an upper limit on the rise time t_{rise} is 26 ps so the particles must oscillate at frequencies f_o of up to at least $f_o = 1/(\pi t_{rise}) \sin^{-1}(0.8) \approx 11$ GHz. This suggests that some fraction of the particles in the specimen must experience an effective field of >3 kOe in the equilibrium magnetization configuration at zero bias field. This expectation is confirmed through inspection of the zero-field initial state of the random array model. For this model the internal fields range from a few tens of Oe to as high as 5 kOe with a mean internal field of 2.5 kOe.

The strong interactions between the nanocrystals also play a role in the slow in-plane switching of the nanocomposite, although in this case, the dynamics are more complex. Although the agreement between simulations and experiment is not complete, some qualitative features are similar. The switching dynamics can be described by two time constants: a fast time constant (10 ns experimentally), which is thought to correspond to the switching of nanocrystals that are relatively free to reorient along the direction of the field, and a slower time constant (300 ns experimentally), which corresponds to slower switching of particles that are pinned through dipolar interactions as well as the overall resettling of the magnetization of the composite into a new equilibrium through damped oscillations of the individual particles.

The importance of dipolar interactions in understanding the magnetic properties of collections of nanoparticles has often been overlooked in the past. In interpreting magnetic hysteresis curves in particular, noninteracting models have been favored for their simplicity. It is only recently^{8,26} that the interparticle interactions have been shown to be neces-

sary for a full understanding of the hysteresis curves for these types of materials. The results presented here indicate that the interactions are not only important in determining the static magnetic properties, but also play a role in defining the characteristics of the dynamic magnetic response. The existence of coercivity at all at room temperature implies the presence of dipolar ferromagnetism as a collection of noninteracting particles the size of those in the specimen would be expected to be superparamagnetic.

VI. CONCLUSIONS

An iron nanocomposite containing a thin layer of strongly interacting Fe nanoparticles was fabricated by implanting 80 keV Fe ions into a SiO₂ host material to a dose of 1.5×10^{17} ions/cm². A large Faraday rotation was observed, and the Verdet constant was found to be 6.3 ± 0.4 /cm/Oe. This yields a minimum Faraday rotation of 3.8 ± 0.2 / μm in a 6 kOe magnetic field, which is still below saturation for this material but is already a larger rotation than a YIG indicator film by more than a factor of six. Although the figure of merit is higher than for bulk iron, it is still too small for conventional magneto-optical applications.

The dynamic properties of the Fe implanted SiO₂ sample were probed using time-resolved Kerr effect microscopy. The in-plane and out-of-plane switching dynamics are quite different with response times as fast as 26 ps observed in the out-of-plane direction. This response is essentially independent of the magnitude of an in-plane bias field up to several kOe, although slight variations in the exact response are observed for excitations with rise times faster than 150 ps. Micromagnetics simulations indicate that the dipolar interactions between single-domain nanoparticles play an important role in influencing the observed dynamic responses.

In conclusion, we have shown that exchange decoupled nanoparticle arrays exhibit a very strong and fast out-of-plane magnetization response. This effect is believed to be a direct consequence of strong dipole interactions between the particles; very little dependence on the particular structure and arrangement of the particles is observed in simulations at these time scales (on the order of pico- to nanoseconds). Micromagnetic simulations consistently demonstrate a fast, linear magnetic response to a transient out-of-plane magnetic field for a wide range of models with different filling factors, randomness of particle placement, distributions of particle sizes and shapes, and the presence or absence of crystalline anisotropy. This fast out-of-plane response is also relatively insensitive to the presence of in-plane magnetic fields. The robust nature of this ultrafast magnetic response may find use in technological applications. We expect that other exchange decoupled nanoparticle arrays will exhibit similar behavior.

ACKNOWLEDGMENTS

We are grateful to C. W. White (Oak Ridge National Laboratory) for providing the implanted specimens and to Xiaobin Zhu for his assistance. The authors acknowledge funding from NSERC and iCORE.

- ¹B. Sepulveda, Y. Huttel, C. Martinez Boubeta, A. Cebollada, and G. Armelles, *Phys. Rev. B* **68**, 064401 (2003).
- ²Z. S. Jiang, G. J. Jin, J. T. Ji, H. Sang, Y. W. Du, S. M. Zhou, Y. D. Wang, and L. Y. Chen, *J. Appl. Phys.* **78**, 439 (1995).
- ³J. L. Menendez, B. Bescos, G. Armelles, R. Serna, J. Gonzalo, R. Doole, A. K. Petford-Long, and M. I. Alonso, *Phys. Rev. B* **65**, 205413 (2002).
- ⁴C. Ross, *Ann. Rev. Mat. Res.* **31**, 203 (2001).
- ⁵Seagate, <http://www.seagate.com/newsinfo/about/milestones/>
- ⁶B. D. Cullity, *Introduction to Magnetic Materials* (Addison-Wesley, Reading, MA, 1972).
- ⁷K. D. Sorge, J. R. Thompson, T. C. Schulthess, F. A. Modine, T. E. Haynes, S. I. Honda, A. Meldrum, J. D. Budai, C. W. White, and L. A. Boatner, *IEEE Trans. Magn.* **37**, 2197 (2001).
- ⁸T. C. Schulthess, M. Benkali, P. B. Visscher, K. D. Sorge, J. R. Thompson, F. A. Modine, T. E. Haynes, L. A. Boatner, G. M. Stocks, and W. H. Butler, *J. Appl. Phys.* **89**, 7594 (2001).
- ⁹R. P. Cowburn and M. E. Welland, *Science* **287**, 1466 (2000).
- ¹⁰M. Freeman and B. C. Choi, *Science* **294**, 1484 (2001).
- ¹¹W. K. Hiebert, Ph.D. thesis, University of Alberta (2001).
- ¹²W. K. Hiebert, A. Stankiewicz, and M. R. Freeman, *Phys. Rev. Lett.* **79**, 1134 (1997).
- ¹³B. C. Choi, M. Belov, W. K. Hiebert, G. E. Ballentine, and M. R. Freeman, *Phys. Rev. Lett.* **86**, 728 (2001).
- ¹⁴A. Meldrum, R. F. J. Haglund, Jr., L. A. Boatner, and C. W. White, *Adv. Mater. (Weinheim, Ger.)* **13**, 1431 (2001).
- ¹⁵K. S. Beaty, A. Meldrum, J. P. Franck, K. Sorge, J. R. Thompson, C. W. White, R. A. Zuhr, L. A. Boatner, and S. Honda, *Mater. Res. Soc. Symp. Proc.* **703**, 331 (2002).
- ¹⁶M. Mansuripur, *Classical Optics and its Applications* (Cambridge University Press, Cambridge, 2002).
- ¹⁷K. S. Buchanan, Ph.D. thesis, University of Alberta (2004).
- ¹⁸M. Freeman and J. Smyth, *J. Appl. Phys.* **79**, 5898 (1996).
- ¹⁹T. Gerrits, H. Hohlfeld, K. J. Gielkens, K. B. Veenstra, and T. Rasing, *J. Appl. Phys.* **89**, 7648 (2001).
- ²⁰D. R. Lide, *CRC Handbook of Chemistry and Physics* (CRC Press, Boca Raton, FL, 2003).
- ²¹G. S. Krinchik and V. A. Artem'ev, *Sov. Phys. JETP* **26**, 1080 (1968).
- ²²M. R. Scheinfein, Landau Lifshitz Gilbert LLG Micromagnetic Simulator™.
- ²³M. J. Freiser, *IEEE Trans. Magn.* **MAG-4**, 152 (1968).
- ²⁴A. K. Zvezdin and V. A. Kotov, *Modern Magneto-optics and Magneto-optical Materials* (Institute of Physics, Bristol, 1997).
- ²⁵C. Kittel, *Phys. Rev.* **73**, 155 (1948).
- ²⁶K. R. Heim, G. G. Hembree, K. E. Schmidt, and M. R. Scheinfein, *Appl. Phys. Lett.* **67**, 2878 (1995).
- ²⁷For a well constrained fit, examining $\sum_i [M_x(t_i) - M_{x,predicted}(t_i)]^2$ will show that the solution is located in a minimum when each parameter is varied. For the four parameter fit used here, however, this is not observed, which suggests that there are correlations between the parameters and that the amplitude and time-constant parameters are not completely independent. The uncertainties listed for the parameters do not reflect the fact that there are other parameter combinations that will describe the data equally as well.